Synthetic Nickel-Containing Heterometal Cubane-Type Clusters with $NiFe_3Q_4$ Cores (Q = S, Se)

Stefano Ciurli, Paul K. Ross,[1] Michael J. Scott, Shi-Bao Yu, and R. H. Holm*

Contribution from the Department of Chemistry, Harvard University, Cambridge, Massachusetts 02138. *Received October 24, 1991*

Abstract: Reaction of the linear trinuclear Fe(III) clusters $[Fe_3Q_4(SEt)_4]^{3-}$ with $Ni(PPh_3)_4$ in acetonitrile solution affords the products $[NiFe_3Q_4(PPh_3)(SEt)_3]^{2-}$ (Q = S (**9**), Se (**10**)) and $[NiFe_3Q_4(SEt)_4]^{3-}$ (Q = S (**11**), Se (**12**)) in ca. 30% yield. The reactions involve reductive rearrangement of the initial cluster to a cuboidal fragment and capture of the nickel atom. The compounds $(Et_4N)_2$[**9**/**10**] are isomorphous and contain cluster anions with the cubane-type $[NiFe_3Q_4]^{1+}$ core units and Ni–PPh_3 and Fe–SEt terminal ligation. The compound $(Et_4N)_3$[**12**] is isomorphous with $(Et_4N)_3[Fe_4Se_4(SEt)_4]$ and contains the same cubane unit but with all-thiolate terminal ligation and disordered Ni and Fe subsites. The dimensions of the $[NiFe_3Q_4]^{1+}$ cores are closely similar to those of the more familiar $[Fe_4Q_4]^{2+,1+}$ cluster cores, rendering separation of the salts of the same cation and cluster charge difficult. Collective structural, magnetic, and spectroscopic results are consistent with the simplified charge distribution $[Fe_3Q_4]^{1-}$ ($S = {}^5/_2$) + Ni^{2+} ($S = 1$) and an $S = {}^3/_2$ ground state that arises from antiparallel coupling of the two fragment spins. This mode of spin coupling causes oppositely signed isotropic shifts of the identical ligands at Ni and Fe subsites. Subsite-differentiated cluster **9** undergoes regiospecific substitution reactions to afford products with phosphines, cyanide, and isonitrile at the Ni subsite. These reactions are often accompanied by formation of $[Fe_4S_4(SEt)_4]^{2-,3-}$ minority products. Comparison of properties of the synthetic clusters and of a reconstituted $NiFe_3S_4$ species formed with *Pyrococcus furiosus* ferredoxin (Conover, R. C.; Park, J.-B.; Adams, M. W.; Johnson, M. K. *J. Am. Chem. Soc.* **1990**, *112*, 4562) reveals that they are isoelectronic with the same ground state. Consequently, the protein-bound species almost certainly has the cubane-type structure of the synthetic cluster. Some seven types of heterometal cubane clusters MFe_3S_4 (M = V, Nb, Mo, W, Re, Co, Ni) have now been prepared. Reductive rearrangement reactions are likely to provide routes to additional members of the set, several of which are good structural models for the immediate heterometal coordination environment in enzymes (M = V, Mo), but none of which has as yet been shown to occur naturally.

Introduction

Clusters containing the heterometal cubane-type core MFe_3S_4 (**1**) with M = V,[2-4] Mo,[4-6] W,[5] and, most recently, Re[7-9] have been synthesized and extensively investigated in this laboratory.

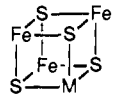

1

Those with M = V and Mo remain of considerable interest because of the structural similarity of the heterometal atom coordination sites and those present in the FeMo and FeV cofactors of nitrogenases.[10] Together with the other clusters containing early transition metals, species with M = Re serve to emphasize further a stability plateau associated with cores having 50–53 e^- and a special stability at 51 e^- and reveal the effects of cluster charge on the redox potentials of isoelectronic clusters. All of these clusters were prepared in self-assembly systems containing the appropriate tetrathiometalate $[MS_4]^{2-}$ as the heterometal and sulfur source.

Recently, it has become apparent that MFe_3S_4 clusters with late transition-metal elements as the heterometal can also be formed. As illustrated schematically in Figure 1, the protein-bound cuboidal cluster $Fe_3S_4(S\text{-}Cys)_3$, when in the $[Fe_3S_4]^{0,1-}$ oxidation state, will bind the indicated divalent "biological" metals to form presumed cubane-type clusters with M = Co,[11] Ni,[12] Zn,[13-15] and Cd.[14,15] These reactions have been pursued principally with the 3-Fe ferredoxin (Fd) proteins *Desulfovibrio gigas* Fd II,[11,13,14] whose cuboidal cluster has been demonstrated by X-ray diffraction,[16] *Pyrococcus furiosus* Fd,[12,17] and the 7-Fe *Desulfovibrio africanus* Fd III.[15,18] Their success emphasizes the concept of the cuboidal Fe_3S_4 fragment as a "semirigid cluster ligand".[9,19]

These results immediately raise the issues of synthetic pathways to those clusters whose heterometals do not form tetrathiometalates and the stabilities of such clusters outside of the potentially beneficial protein structure. We have recently shown that cubane-type $NiFe_3Q_4$ clusters (Q = S, Se) can be prepared,[20] and shortly thereafter, Jordanov and co-workers[21] reported a $CoFe_3S_4$ cluster.[22] These results, we believe, presage entry to an even more diverse set of MFe_3S_4 clusters than currently exists. The current status of the synthesis and reactions of these clusters has been

(1) NIH Postdoctoral Fellow, 1990–1992.
(2) Kovacs, J. A.; Holm, R. H. *Inorg. Chem.* **1987**, *26*, 702, 711.
(3) Carney, M. J.; Kovacs, J. A.; Zhang, Y.-P.; Papaefthymiou, G. C.; Spartalian, K.; Frankel, R. B.; Holm, R. H. *Inorg. Chem.* **1987**, *26*, 719.
(4) Ciurli, S.; Holm, R. H. *Inorg. Chem.* **1989**, *28*, 1685.
(5) Holm, R. H.; Simhon, E. D. In *Molybdenum Enzymes*; Spiro, T. G., Ed.; Wiley-Interscience: New York, 1985; Chapter 2.
(6) Zhang, Y.-P.; Bashkin, J. K.; Holm, R. H. *Inorg. Chem.* **1987**, *26*, 694.
(7) Ciurli, S.; Carney, M. J.; Papaefthymiou, G. C.; Holm, R. H. *Inorg. Chem.* **1989**, *28*, 2696.
(8) Ciurli, S.; Carrié, M.; Holm, R. H. *Inorg. Chem.* **1990**, *29*, 3493.
(9) Ciurli, S.; Holm, R. H. *Inorg. Chem.* **1991**, *30*, 743.
(10) Burgess, B. K. *Chem. Rev.* **1990**, *90*, 1377.
(11) Moura, I.; Moura, J. J. G.; Münck, E.; Papaefthymiou, V.; LeGall, J. *J. Am. Chem. Soc.* **1986**, *108*, 349.
(12) Conover, R. C.; Park, J.-B.; Adams, M. W. W.; Johnson, M. K. *J. Am. Chem. Soc.* **1990**, *112*, 4562.
(13) Surerus, K. K.; Münck, E.; Moura, I.; Moura, J. J. G.; LeGall, J. *J. Am. Chem. Soc.* **1987**, *109*, 3805.
(14) Münck, E.; Papaefthymiou, V.; Surerus, K. K.; Girerd, J.-J. In *Metal Ions in Proteins*; Que, L., Jr., Ed.; ACS Symposium Series 372; American Chemical Society: Washington, DC, 1988; Chapter 15.
(15) Butt, J. N.; Armstrong, F. A.; Breton, J.; George, S. J.; Thomson, A. J.; Hatchikian, E. C. *J. Am. Chem. Soc.* **1991**, *113*, 6663.
(16) (a) Kissinger, C. R.; Adman, E. T.; Sieker, L. C.; Jensen, L. H. *J. Am. Chem. Soc.* **1988**, *110*, 8721. (b) Kissinger, C. R.; Sieker, L. C.; Adman, E. T.; Jensen, L. H. *J. Mol. Biol.* **1991**, *219*, 693.
(17) Conover, R. C.; Finnegan, M. G.; Park, J.-B.; Adams, M. W. W.; Johnson, M. K. *Abstr. Fifth Int. Conf. Bioinorg. Chem.*; *J. Inorg. Biochem.* **1991**, *43*, 245.
(18) Butt, J. N.; Sucheta, A.; Armstrong, F. A.; Breton, J.; Thomson, A. J.; Hatchikian, E. C. *J. Am. Chem. Soc.* **1991**, *113*, 8948. In this work, it is shown that Tl^+ binds (weakly) to the $[Fe_3S_4]^{1+}$ state, indicating that a soft (thiophilic) metal may coordinate to the fully oxidized cuboidal cluster.
(19) Holm, R. H. *Adv. Inorg. Chem.*, in press.
(20) Ciurli, S.; Yu, S.-B.; Holm, R. H.; Srivastava, K. K. P.; Münck, E. *J. Am. Chem. Soc.* **1990**, *112*, 8169.
(21) Roth, E. K. H.; Greneche, J. M.; Jordanov, J. *J. Chem. Soc., Chem. Commun.* **1991**, 105. tibt = 2,4,6-triisopropylbenzenethiolate(1−).
(22) We have prepared $CoFe_3S_4$ clusters by a different method: Zhou, J.; Scott, M. J.; Peng, G.; Holm, R. H. Unpublished results.

0002-7863/92/1514-5415$03.00/0

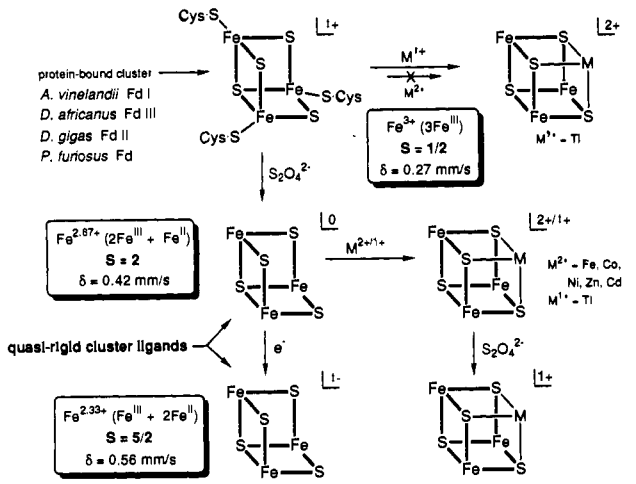

Figure 1. Schematic representation of the binding of divalent metal ions to the cuboidal Fe_3S_4 cluster in proteins. Isomer shifts[43] and spin states[18,43-45] of the $[Fe_3S_4]^{1+,0,1-}$ cluster oxidation states are indicated.

analyzed.[19] Here we describe the synthesis, structures, and electronic and reactivity properties of $NiFe_3Q_4$ species, the first heterometal cubane-type cluster of a late transition-metal element to be examined in detail. As will be seen, certain properties of these clusters support the formation of a protein-bound cubane-type $NiFe_3S_4$ cluster.[12]

Experimental Section

Preparation of Compounds. All operations were conducted under a pure dinitrogen atmosphere using standard Schlenk techniques or an inert atmosphere box. Acetonitrile was distilled from CaH_2 and stored over 4-Å molecular sieves. Ether and THF were distilled from sodium–benzophenone and acetone and 2-butanone from calcium sulfate. All solvents were thoroughly degassed before use, and NMR solvents were dried over 4-Å molecular sieves. Volume reduction and drying steps were performed in vacuo at ambient temperature.

$(Et_4N)_2[NiFe_3S_4(PPh_3)(SEt)_3]$. A mixture of 2.5 g (2.3 mmol) of $Ni(PPh_3)_4$[23] and 2.0 g (2.2 mmol) of $(Et_4N)_3[Fe_3S_4(SEt)_4]$[24] in 80 mL of acetonitrile was stirred overnight. A solution of 0.15 g (0.59 mmol) of iodine in 25 mL of acetonitrile was introduced dropwise to the rapidly stirred reaction mixture, followed by the addition of 80 mL of toluene. The mixture was stirred for 18 h and filtered, and the filtrate was evaporated to dryness. The residue was washed with 25 mL of 2-butanone and redissolved in 300 mL of acetone. This solution was warmed to 45 °C and filtered, and the volume of the filtrate was reduced to 75 mL. Addition of 125 mL of ether caused separation of a black solid, which was collected by filtration, washed with 2-butanone (3 × 50 mL), ether (2 × 40 mL), and dried to afford 0.65 g (29%) of pure product. An analytical sample was recrystallized from acetonitrile/ether. Anal. Calcd for $C_{40}H_{70}Fe_3N_2NiPS_7$: C, 45.30; H, 6.65; Fe, 15.80; N, 2.64; Ni, 5.53; P, 2.81; S, 21.16. Found: C, 44.88; H, 6.62; Fe, 16.46; N, 2.55; Ni, 5.23; P, 2.81; S, 22.79. ^1H NMR (CD_3CN, 293 K, anion): δ 4.16 (*m*-H), 4.32 (SCH_2CH_3), 9.17 (*o*-H), 10.84 (*p*-H), 58.2 (SCH_2CH_3).

$(Et_4N)_3[MFe_3S_4(SEt)_4]$ (M = Ni/Fe). A mixture of 2.0 g (1.8 mmol) of $Ni(PPh_3)_4$ and 1.6 g (1.7 mmol) of $[Et_4N]_3[Fe_3S_4(SEt)_4]$ in 50 mL of acetonitrile was stirred overnight. Toluene (50 mL) was added to the mixture, which was allowed to stand for 24 h and then filtered, and the filtrate was evaporated to dryness. The residue was washed with 70 mL of toluene, dried, and redissolved in 40 mL of acetonitrile. The solution was filtered, and the volume was reduced to 25 mL. Ether (75 mL) was added to the solution, which was maintained at 0 °C overnight and filtered. The solid collected by filtration was washed with ether (2 × 25 mL) and dried, yielding 0.76 g (45%) of black solid. The product typically consists of a mixture of ca. 70% $(Et_4N)_3[NiFe_3S_4(SEt)_4]$ and 30% $(Et_4N)_3[Fe_4S_4(SEt)_4]$ from ^1H NMR analysis. Attempts to improve this ratio by recrystallization proved to be unsuccessful. ^1H NMR (CD_3CN, 293 K, Ni anion): δ −39.4 ($NiSCH_2$), 5.87 ($FeSCH_2CH_3$), 58.4 ($FeSCH_2$). The spectrum of $[Fe_4S_4(SEt)_4]^{3-}$ has been reported elsewhere.[25]

$(Et_4N)_2[NiFe_3Se_4(PPh_3)(SEt)_3]$. A mixture of 0.63 g (0.71 mmol) of $Ni(PPh_3)_4$ and 0.75 g (0.68 mmol) of $(Et_4N)_3[Fe_3Se_4(SEt)_4]$[26] in 35 mL of acetonitrile was stirred overnight and filtered. Solvent was removed and the residue was dissolved in 150 mL of acetone. The solution was filtered, and the filtrate was reduced in volume to 50 mL. Ether (100 mL) was added, and the solution was stored at −20 °C overnight. The solid was collected by filtration, washed with ether, and dried to give 0.22 g (27%) of pure product as a black microcrystalline solid. Anal. Calcd for $C_{40}H_{70}Fe_3N_2NiPS_3Se_4$: C, 38.49; H, 5.65; Fe, 13.42; N, 2.24; Ni, 4.70; P, 2.48; S, 7.71; Se, 25.30. Found: C, 38.62; H, 5.30; Fe, 13.08; N, 2.20; Ni, 4.65; P, 2.79; S, 7.78; Se, 25.43. ^1H NMR (CD_3CN, 293 K, anion): δ 3.80 (SCH_2CH_3), 4.15 (*m*-H), 9.35 (*o*-H), 11.20 (*p*-H), 63.0 (SCH_2CH_3). UV (CH_3CN): λ_{max} (ϵ_M) 313 (21 500), 397 nm (16 600).

$(Et_4N)_3[NiFe_3Se_4(SEt)_4]$. A solution of 0.84 g (0.94 mmol) of $Ni(PPh_3)_4$ in 50 mL of THF was added dropwise to a solution of 1.0 g (0.90 mmol) of $(Et_4N)_3[Fe_3Se_4(SEt)_4]$[26] in 50 mL of acetonitrile. The solution was stirred for 5 h and filtered, and the filtrate was evaporated to dryness. The resulting black residue was washed thoroughly with toluene and ether and was redissolved in acetonitrile. Ether was added to this solution, resulting in the precipitation of black microcrystals which were collected by filtration, washed with ether, and dried to afford 0.35 g (30%) of product. While the compound was obtained in satisfactory analytical purity, ^1H NMR usually revealed small amounts of $(Et_4N)_3[Fe_4Se_4(SEt)_4]$ or $(Et_4N)_2[Fe_4Se_4(SEt)_4]$.[26] Anal. Calcd for $C_{32}H_{80}Fe_3N_3NiS_4Se_4$: C, 32.65; H, 6.85; Fe, 14.23; N, 3.57; Ni, 4.99; S, 10.89; Se, 26.83. Found: C, 32.56; H, 6.18; Fe, 14.47; N, 3.64; Ni, 4.25; S, 9.69; Se, 27.30. ^1H NMR (CD_3CN, 293 K, anion): δ −42.4 ($NiSCH_2$), 6.30 ($FeSCH_2CH_3$), 62.0 ($FeSCH_2$). UV (CH_3CN): λ_{max} (ϵ_M) 314 (sh, 17 500), 390 nm (sh, 11 900).

Generation of Clusters in Solution. A series of clusters $[NiFe_3S_4(SEt)_3L]^{z-}$ was prepared in situ by substitution of PPh_3 in $[NiFe_3S_4(PPh_3)(SEt)_3]^{2-}$ with ligands $L^{0,1-}$. In a typical experiment, a known amount of ligand in CD_3CN was added to a ca. 15 mM solution of the cluster in the same solvent. Reactions were immediate and were monitored by ^1H NMR.

X-ray Data Collection and Reduction. Black crystals of compounds 9, **10**, and **12** in Table I were grown by vapor diffusion of ether into a saturated solution of the compounds in acetone (9) or acetonitrile (**10**, **12**). (See compound numbering scheme below.) Single crystals of 9 and **10** were mounted in glass capillaries while a suitable crystal of **12** was coated with grease and attached to a glass fiber. The crystals were then transferred to a Nicolet P3F (9, **10**) or R3 (**12**) diffractometer equipped with a low-temperature device. Lattice parameters were obtained from a least-squares analysis of 50 (**9**, **10**) or 23 (**12**) machine-centered reflections with $15° \le 2\theta \le 30°$. Decay corrections were based on the measured intensities of three reflections monitored periodically throughout the course of data collection, and only 9 showed significant decay (ca. 20%). The raw intensity data were converted to structure factor amplitudes and their esd's by correction for scan speed, background, and Lorentz and polarization effects using the program XDISK of the SHELXTL PLUS program package. An empirical absorption correction based on the observed variation in intensity of azimuthal (Ψ)

Table I. Crystallographic Data[a] for $(Et_4N)_2[NiFe_3S_4(PPh_3)(SEt)_3]$ (9), $(Et_4N)_2[NiFe_3Se_4(PPh_3)(SEt)_3]$ (**10**), and $(Et_4N)_3[NiFe_3Se_4(SEt)_4]$ (**12**)

	9	10	12
formula	$C_{40}H_{70}Fe_3N_2NiPS_7$	$C_{40}H_{70}Fe_3N_2NiPS_3Se_4$	$C_{32}H_{80}Fe_3N_3NiS_4Se_4$
formula wt	1060.6	1248.3	1177.4
cryst system	monoclinic	monoclinic	monoclinic
space group	$P2_1/n$	$P2_1/n$	$P2_1/n$
Z	4	4	4
a, Å	13.338 (5)	13.467 (3)	11.596 (2)
b, Å	14.657 (7)	14.353 (2)	36.768 (6)
c, Å	26.627 (9)	27.112 (4)	11.849 (2)
β, deg	100.46 (3)	102.20 (1)	106.79 (2)
V, Å^3	5119 (3)	5122 (2)	4836 (2)
d_{calc} (d_{obs}), g/cm^3	1.38 (1.39[b])	1.62 (1.59[c])	1.62 (1.59[c])
T, K	298	298	193
μ, cm^{-1}	15.3	39.3	41.7
R,[d] R_w[e] (%)	9.5, 10.3	5.33, 6.17	4.45, 6.07

[a] All data collected with Mo Kα radiation (λ = 0.710 69 Å). [b] Determined by the neutral buoyancy in carbon tetrachloride/hexane. [c] Determined by the neutral buoyancy in 1,3-dibromopropane/hexane. [d] $R = \sum||F_o| - |F_c||/\sum|F_o|$. [e] $R_w = [\sum[w(|F_o| - |F_c|^2)]/\sum[w|F_o|^2]]^{1/2}$.

(23) Ittel, S. D. *Inorg. Synth.* **1990**, *28*, 102.
(24) Hagen, K. S.; Watson, A. D.; Holm, R. H. *J. Am. Chem. Soc.* **1983**, *105*, 3905.
(25) Hagen, K. S.; Watson, A. D.; Holm, R. H. *Inorg. Chem.* **1984**, *23*, 2984.
(26) Yu, S.-B.; Papaefthymiou, G. C.; Holm, R. H. *Inorg. Chem.* **1991**, *30*, 3476.

Table II. Selected Interatomic Distances (Å) and Bond Angles (deg) for $[NiFe_3Q_4(PPh_3)(SEt)_3]^{2-}$

Q = S		Q = Se	
Ni-Fe(1)	2.691 (4)	Ni-Fe(1)	2.730 (2)
Ni-Fe(2)	2.672 (4)	Ni-Fe(2)	2.723 (2)
Ni-Fe(3)	2.704 (5)	Ni-Fe(3)	2.712 (2)
mean	2.69 (2)	mean	2.722 (2)
Fe(1)-Fe(2)	2.773 (5)	Fe(1)-Fe(2)	2.789 (2)
Fe(1)-Fe(3)	2.743 (5)	Fe(1)-Fe(3)	2.798 (2)
Fe(2)-Fe(3)	2.749 (5)	Fe(2)-Fe(3)	2.829 (2)
mean	2.755 (16)	mean	2.81 (2)
Ni-S(1)	2.268 (7)	Ni-Se(1)	2.385 (1)
Ni-S(2)	2.255 (7)	Ni-Se(2)	2.380 (1)
Ni-S(3)	2.262 (6)	Ni-Se(3)	2.367 (1)
mean	2.262 (6)	mean	2.377 (9)
Ni···S(4)	3.824 (7)	Ni···Se(4)	3.987 (2)
Fe(1)-S(2)	2.298 (7)	Fe(1)-Se(2)	2.396 (2)
Fe(1)-S(3)	2.267 (7)	Fe(1)-Fe(3)	2.421 (2)
Fe(2)-S(1)	2.274 (7)	Fe(2)-Se(1)	2.397 (2)
Fe(2)-S(3)	2.281 (7)	Fe(2)-Se(3)	2.423 (2)
Fe(3)-S(1)	2.269 (7)	Fe(3)-Se(1)	2.405 (2)
Fe(3)-S(2)	2.306 (8)	Fe(3)-Se(2)	2.416 (2)
mean	2.282 (16)	mean	2.41 (1)
Fe(1)-S(4)	2.287 (8)	Fe(1)-Se(4)	2.429 (2)
Fe(2)-S(4)	2.302 (8)	Fe(2)-Se(4)	2.399 (2)
Fe(3)-S(4)	2.301 (7)	Fe(3)-Se(4)	2.435 (2)
mean	2.2967 (8)	mean	2.42 (2)
Ni-P	2.174 (6)	Ni-P	2.172 (2)
Fe(1)-S(5)	2.282 (7)	Fe(1)-S(1)	2.280 (3)
Fe(2)-S(6)	2.289 (9)	Fe(2)-S(2)	2.283 (3)
Fe(3)-S(7)	2.278 (8)	Fe(3)-S(3)	2.283 (3)
mean	2.283 (6)	mean	2.282 (2)
S(1)-Ni-S(2)	105.1 (3)	Se(1)-Ni-Se(2)	109.2 (1)
S(1)-Ni-S(3)	106.5 (2)	Se(1)-Ni-Se(3)	108.4 (1)
S(2)-Ni-S(3)	105.7 (2)	Se(2)-Ni-Se(3)	107.4 (I)
Fe(1)-Ni-Fe(2)	62.3 (1)	Fe(1)-Ni-Fe(2)	61.5 (1)
Fe(1)-Ni-Fe(3)	61.1 (1)	Fe(1)-Ni-Fe(3)	61.9 (1)
Fe(2)-Ni-Fe(3)	61.5 (1)	Fe(2)-Ni-Fe(3)	62.7 (1)
Ni-Fe(1)-Fe(2)	58.5 (1)	Ni-Fe(1)-Fe(2)	59.1 (1)
Ni-Fe(1)-Fe(3)	59.7 (1)	Ni-Fe(1)-Fe(3)	58.7 (1)
Ni-Fe(2)-Fe(1)	59.2 (1)	Ni-Fe(2)-Fe(1)	59.4 (1)
Ni-Fe(2)-Fe(3)	59.8 (1)	Ni-Fe(2)-Fe(3)	58.4 (1)
Ni-Fe(3)-Fe(1)	59.2 (1)	Ni-Fe(3)-Fe(1)	59.4 (1)
Ni-Fe(3)-Fe(2)	58.7 (1)	Ni-Fe(3)-Fe(2)	58.6 (1)
Ni-S(1)-Fe(2)	72.1 (2)	Ni-Se(1)-Fe(2)	69.4 (1)
Ni-S(1)-Fe(3)	73.2 (2)	Ni-Se(1)-Fe(3)	69.0 (1)
Ni-S(2)-Fe(1)	72.5 (2)	Ni-Se(2)-Fe(1)	69.7 (1)
Ni-S(2)-Fe(3)	72.7 (2)	Ni-Se(2)-Fe(3)	68.9 (1)
Ni-S(3)-Fe(1)	72.9 (2)	Ni-Se(3)-Fe(1)	69.5 (1)
Ni-S(3)-Fe(2)	72.1 (2)	Ni-Se(3)-Fe(2)	69.3 (1)
S(2)-Fe(1)-S(3)	104.1 (2)	Se(2)-Fe(1)-Se(3)	105.2 (1)
S(1)-Fe(2)-S(3)	105.7 (2)	Se(1)-Fe(2)-Se(3)	106.2 (1)
S(1)-Fe(3)-S(2)	103.4 (3)	Se(1)-Fe(3)-Se(2)	107.4 (1)
S(2)-Fe(1)-S(4)	105.3 (3)	Se(2)-Fe(1)-Se(4)	107.1 (1)
S(3)-Fe(1)-S(4)	103.1 (3)	Se(2)-Fe(1)-Se(4)	106.5 (1)
S(1)-Fe(2)-S(4)	103.9 (3)	Se(1)-Fe(2)-Se(4)	105.2 (1)
S(3)-Fe(2)-S(4)	102.2 (3)	Se(3)-Fe(2)-Se(4)	107.4 (1)
S(1)-Fe(3)-S(4)	104.1 (3)	Se(1)-Fe(3)-Se(4)	103.9 (1)
S(2)-Fe(3)-S(4)	104.6 (3)	Se(2)-Fe(3)-Sc(4)	106.2 (1)
S(4)-Fe(1)-S(5)	109.8 (3)	Se(4)-Fe(1)-S(2)	105.3 (1)
S(4)-Fe(2)-S(6)	114.3 (3)	Se(4)-Fe(2)-S(3)	107.9 (1)
S(4)-Fe(3)-S(7)	109.7 (3)	Se(4)-Fe(3)-S(4)	114.0 (1)
Fe(2)-S(1)-Fe(3)	74.5 (2)	Fe(2)-Se(1)-Fe(3)	72.2 (1)
Fe(1)-S(2)-Fe(3)	73.1 (2)	Fe(1)-Se(2)-Fe(3)	71.1 (1)
Fe(1)-S(3)-Fe(2)	75.2 (2)	Fe(1)-Se(3)-Fe(2)	70.3 (1)
Fe(1)-S(4)-Fe(2)	74.4 (2)	Fe(1)-Fe(4)-Fe(2)	70.6 (1)
Fe(1)-S(4)-Fe(3)	73.5 (2)	Fe(1)-Se(4)-Fe(3)	70.2 (1)
Fe(2)-S(4)-Fe(3)	73.3 (2)	Fe(2)-Se(4)-Fe(3)	71.6 (1)
Fe(1)-Ni-P	141.7 (2)	Fe(1)-Ni-P	145.9 (1)
Fe(2)-Ni-P	143.5 (2)	Fe(2)-Ni-P	139.8 (1)
Fe(3)-Ni-P	145.9 (2)	Fe(3)-Ni-P	144.6 (1)
S(1)-Ni-P	115.3 (2)	Se(1)-Ni-P	109.0 (1)
S(2)-Ni-P	112.0 (2)	Se(2)-Ni-P	114.2 (1)
S(3)-Ni-P	111.6 (2)	Se(3)-Ni-P	108.3 (1)

scans was applied to all of the data sets using the program XEMP. The three compounds crystallized in the monoclinic system, and the systematic absences ($0k0$, $k = 2n + 1$; $h0l$, $h + l = 2n + 1$) identified the space group as $P2_1/n$ for all three structures. Crystallographic data are contained in Table I.

Structure Solutions and Refinements. The structures of **10** and **12** were solved by direct methods, and the heavy atom coordinates of **10** were used as starting parameters for the refinement of the isomorphous compound **9**. The structures were refined by means of standard least-squares and Fourier techniques, and all non-hydrogen atoms were refined with anisotropic thermal parameters unless otherwise noted. Hydrogen atoms were assigned idealized locations and given a uniform value for B_{iso} of 0.8 Å^2.

The asymmetric units of **9** and **10** consist of one cluster anion and two cations. In **9**, the phenyl rings of the phosphine were treated as rigid, regular hexagons with a fixed distance of 1.395 Å between carbon atoms. The cation carbon atoms showed a great deal of thermal motion and were refined isotropically. Also, in **9**, the terminal methyl groups of the cation and thiolate carbon atoms were refined with a fixed thermal parameter. In **10**, the methyl groups of two thiolate ligands were disordered over two positions and were refined with 0.5 occupancy factor. The asymmetric unit of **12** consists of one cluster anion and three cations. No unique site could be found for the nickel atom, and the cluster was refined with each metal site having the occupancies of 0.75 Fe and 0.25 Ni. Attempted refinement of the structure as an Fe_4S_4 cluster converged to a higher R value than for the $NiFe_3S_4$ cluster refinement. In the last cycles of refinement of the three structures, all parameters shifted by <1% of their esd's, and final difference Fourier maps showed no significant electron density. Structural data are available in Table II and elsewhere.[27]

Other Physical Measurements. Spectrophotometric, spectroscopic, electrochemical, and magnetic measurements were performed under anaerobic conditions using the equipment and procedures described earlier.[9,28] Cyclic voltammetry measurements in acetonitrile solutions were carried out at a scan rate of 50 mV/s with use of a Pt disk working electrode, 0.1 M $(Bu_4N)X$ ($X = ClO_4^-$, PF_6^-) supporting electrolyte, and a SCE reference electrode. Magnetic susceptibility measurements were made at 5 kOe with a SHE SQUID susceptometer operating at 1.8–300 K. EPR spectra were recorded at X-band frequencies on a Varian Model E109 spectrometer.

Results and Discussion

The following clusters are of principal interest in this work. The structures of all clusters but **11** and **13** have been determined by X-ray crystallography; those of **2–4**, **8**, and **9–12** are schematically depicted in Figure 2.

	Q = S	Se
$[Fe_3Q_4(SEt)_4]^{3-}$	**2**	**3**
$[Fe_4Q_4(SEt)_4]^{2-}$	**4**	**5**
$[Fe_4Q_4(SEt)_4]^{3-}$	**6**	**7**
$[MoFe_3S_4(CO)_3(SEt)_3]^{3-}$	**8**	
$[NiFe_3Q_4(PPh_3)(SEt)_3]^{2-}$	**9**	**10**
$[NiFe_3Q_4(SEt)_4]^{3-}$	**11**	**12**
$[CoFe_3S_4(tibt)_4]^{2-}$	**13**	

Preparation of Compounds. In the absence of a suitable thionickelate or a stable synthetic cuboidal Fe_3S_4 cluster, a new preparative route to $NiFe_3Q_4$ clusters (Q = S, Se) was required. The successful method is based on prior reactions 1[24] and 2,[29]

$$[Fe_3S_4(SEt)_4]^{3-} + FeCl_2 + EtS^- \rightarrow [Fe_4S_4(SEt)_4]^{2-} + 2Cl^- + \tfrac{1}{2}EtSSEt \quad (1)$$

$$[Fe_3S_4(SEt)_4]^{3-} + Mo(CO)_3(MeCN)_3 \rightarrow [MoFe_3S_4(CO)_3(SEt)_3]^{3-} + \tfrac{1}{2}EtSSEt \quad (2)$$

which are illustrated in Figure 2; product clusters were isolated

(27) See the paragraph at the end of this article concerning supplementary material available.

(28) Ciurli, S.; Carrié, M.; Weigel, J. A.; Carney, M. J.; Stack, T. D. P.; Papaefthymiou, G. C.; Holm, R. H. *J. Am. Chem. Soc.* **1990**, *112*, 2654.

(29) Coucouvanis, D.; Al-Ahmad, S.; Salifoglou, A.; Dunham, W. R.; Sands, R. H. *Angew. Chem., Int. Ed. Engl.* **1988**, *27*, 1353.

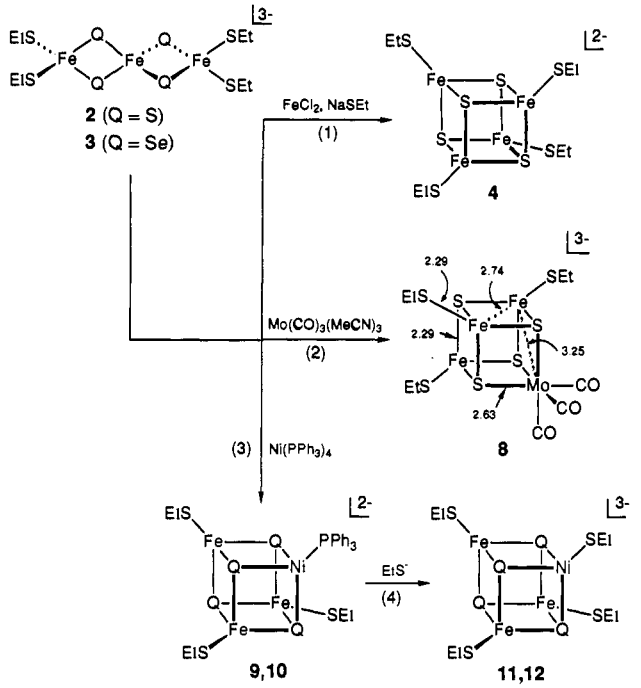

Figure 2. Synthesis of the heterometal cubane-type clusters **4** and **8–12** by reductive rearrangement of trinuclear precursor clusters **2** and **3**. Clusters **9–12** were prepared in this work.

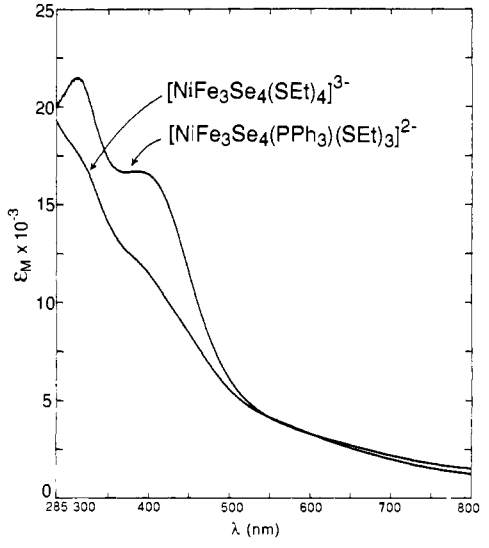

Figure 3. Absorption spectra of clusters **10** and **12** in acetonitrile solutions.

as R_4N^+ salts in ca. 60% yield. These reactions demonstrate the key point that the $[Fe_3S_4]^{1+}$ core of the linear trinuclear cluster **2**[24] can be induced to rearrange to a cuboidal form upon reduction and capture of a metal atom to complete the cubane-type structure. In the context of Figure 1, the core is reduced by thiolate to $[Fe_3S_4]^0$, which then binds Fe(II) or Mo(0). In the latter case, the $[MoFe_3S_4]^0$ core of **8** displays a trigonal elongation reflected in the long Mo–S and Mo–Fe mean distances. While the molybdenum atom is not tightly integrated into the core, the cubane-type structure of the Fe_3S_4 fragment is apparent.[30]

The foregoing results form the basis for the successful synthesis of $NiFe_3Q_4$ clusters **9** and **10** by reaction 3. Here, Ni(0) is the apparent reductant in an inner-sphere process which we conceive of as involving concerted reductive rearrangement of the trinuclear precursor **2**/**3** and capture of oxidized nickel. Given the dissociative lability of $Ni(PPh_3)_4$,[31] the actual reactant is likely coordinatively unsaturated $Ni(PPh_3)_3$, whose trigonal planar structure has recently been demonstrated.[32] Indeed, our initial preparations of **9** and **10** employed this compound.[20] Two clusters are isolated from the reaction mixtures in *separate* workups: phosphine clusters **9**/**10** and the all-thiolate clusters **11**/**12**. The latter are presumably formed in reaction 4 after free PPh_3 pro-

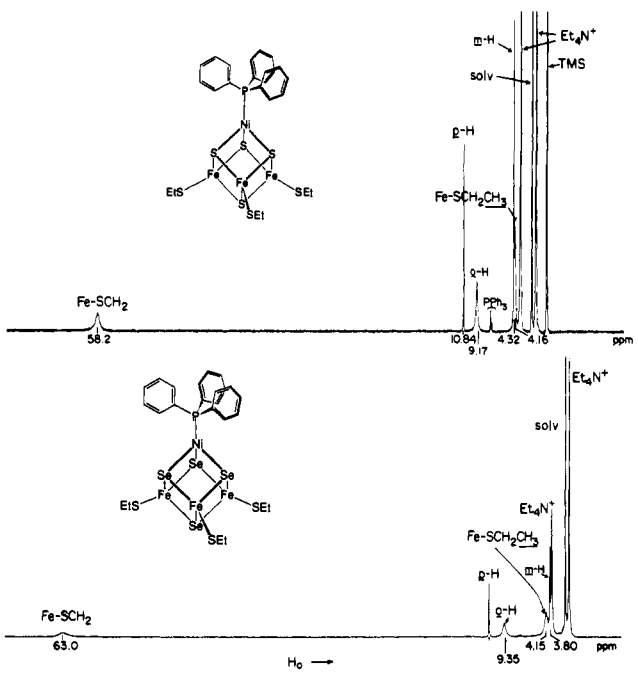

Figure 4. ^1H NMR spectra of clusters **9** and **10** in CD_3CN solutions at 293 K; signal assignments are indicated.

$$[Fe_3Q_4(SEt)_4]^{3-} + Ni(PPh_3)_4 \rightarrow [NiFe_3S_4(PPh_3)(SEt)_3]^{2-} + 3PPh_3 + EtS^- \quad (3)$$

$$[NiFe_3S_4(PPh_3)(SEt)_3]^{2-} + EtS^- \rightarrow [NiFe_3S_4(SEt)_4]^{3-} + PPh_3 \quad (4)$$

duced in reaction 3 is removed by treatment with toluene.[33] The reaction systems also produce varying amounts of the reduced Fe_4Q_4 clusters **6**/**7**, which were detected by ^1H NMR.[25,26] The formation of mixed products and the necessity to resolve them by solubility differences accounts for purified yields of ca. 30%.

In the Q = S reaction system, the similar solubility properties of the Et_4N^+ salts of **6**, **9**, and **11** precluded their separation by fractional crystallization. However, treatment of the mixture with iodine caused oxidation of **6** to **4**[34] and conversion of the small amount of **11** formed to **4**. $(Et_4N)_2$[**4**] was removed from the product mixture by extraction with 2-butanone, allowing the isolation of $(Et_4N)_2$[**9**] in 29% yield. Cluster **11** was never obtained free of the Fe_4S_4 cluster **6**, whose Et_4N^+ salts cocrystallize and could not be separated by fractional recrystallization. Typically, the clusters were isolated in the approximate mole ratio **11**:**6** ≈ 7:3.

(30) In conventional clusters with the $[MoFe_3S_4]^{3+}$ oxidation level,[5] Mo–S and Mo–Fe distances occur in the ranges 2.3–2.4 and 2.7–2.8 Å, respectively.

(31) Tolman, C. A.; Seidel, W. C.; Gerlach, D. H. *J. Am. Chem. Soc.* **1972**, *94*, 2669.

(32) Dick, D. G.; Stephan, D. W.; Campana, C. W. *Can. J. Chem.* **1990**, *68*, 628.

(33) The washing of solid residues in the preparation of $(Et_4N)_3$[**11**] and $(Et_4N)_3$[**12**] removes uncoordinated PPh_3, facilitating the substitution of bound phosphine by EtS^-. We have also ascertained that the compounds $Ni(PPh_2Me)_4$ and $Ni(PPhMe_2)_4$[23] serve as precursors to phosphine and all-thiolate clusters in reactions analogous to reactions 3 and 4. The reaction of $Ni(AsPh_3)_4$[23] with **2** gave **11**, with no indication of an arsine-ligated cluster. Apparently, any bound $AsPh_3$ is very easily displaced by EtS^-. Because this reaction system affords appreciable quantities of **6**, it offers no advantage over reactions 3 and 4 in the preparation of cluster mixtures enriched in **11**.

(34) $E_{1/2}$ values (vs SCE) in acetonitrile: $[Fe_4S_4(SEt)_4]^{3-/2-}$, −1.29 V; $[NiFe_3S_4(SEt)_4]^{3-/2-}$, −0.96 V.

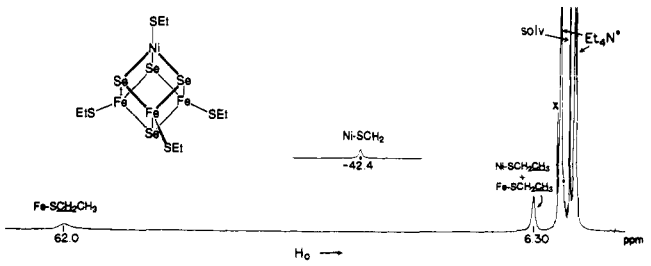

Figure 5. ^{1}H NMR spectrum of cluster **12** in CD_3CN solution at 293 K; signal assignments are indicated.

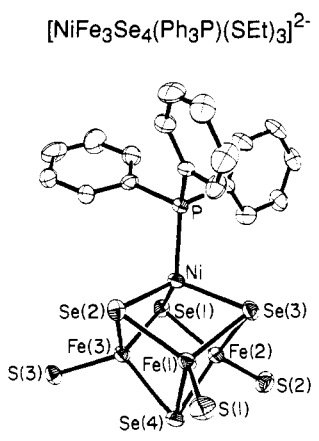

Figure 6. Structure of cluster **10** showing the atom-labeling scheme and 50% probability ellipsoids. A depiction of the structure of cluster **9**, which is essentially isostructural with **10**, has been given earlier.[19]

In the Q = Se reaction system, solubility relationships are more favorable. The compounds $(Et_4N)_3$[**7**] and $(Et_4N)_2$[**10**] were readily separated by fractional recrystallization in acetone/ether, allowing isolation of the latter in 27% yield. It was also possible to obtain $(Et_4N)_3$[**12**] free of significant quantities of $(Et_4N)_3$[**7**] and other contaminants. Fractional crystallization from acetonitrile/ether afforded this compound in 30% yield.

The $NiFe_3Se_4$ clusters **10** and **12** may be recognized by their absorption spectra, shown in Figure 3; spectra of the corresponding $NiFe_3S_4$ species (not shown) are less distinctive. The phosphine clusters **9** and **10** are best characterized by their isotropically shifted ^{1}H NMR spectra, shown in Figure 4, which also convey the substantial purity of the preparations. Spectra of all preparations of **9** contained weak signals near 7 ppm arising from free PPh_3. Inasmuch as we could not completely eliminate these signals by washing the compound extensively with toluene, it is likely that there is a slight amount of free phosphine in equilibrium with the cluster. Free phosphine was barely detectable in the spectra of preparations of **10**. The isolation of essentially pure cluster **12** is demonstrated by the ^{1}H NMR spectrum in Figure 5; only the isotropically shifted signals of this cluster are observed.

Structures. (a) $[NiFe_3Q_4(PPh_3)(SEt)_3]^{2-}$. The compounds $(Et_4N)_2$[**9**] and $(Et_4N)_2$[**10**] crystallize in the space group $P2_1/n$ with no imposed symmetry. The two compounds are isomorphous (Table I), and their clusters are isostructural with the cubane-type stereochemistry **1** established earlier for M = V, Mo, W, and Re compounds. The structures closely approach trigonal symmetry. Selected metric data are contained in Table II, and the structure of **10** is presented in Figure 6. Compared to $[MFe_3S_4]^{2+,3+}$ [2-9] and $[Fe_4Q_4]^{1+,2+}$ [26,35,36] clusters, Fe–Fe and Fe–Q bond distances as well as angles within the $[NiFe_3Q_4]^+$ cores are unexceptional. The cores have assumed a small trigonal distortion whereby the nickel atom is at a smaller perpendicular distance from its adjacent Q_3 and Fe_3 planes than are the three Fe atoms and exhibits a shorter diagonal Ni···Q(4) distance. For example, in **9** the distances are 0.883 Å (to plane S(1–3)) and 2.169 Å (to plane Fe(1–3)), compared to 0.94–0.95 and 2.24–2.25 Å for Fe(1–3) from their Q_3 and Fe_3 planes, respectively. In **10**, the diagonal distance is 3.987 (2) Å, whereas in **5** and **7** the mean diagonal distances are 4.09 (2) and 4.12 (2) Å, respectively. The structural features of principal interest are bond lengths to terminal ligands and their relationship to formal charge distributions of the $[NiFe_3S_4]^{1+}$ core fragments Ni + Fe_3S_4.

The Fe–SEt mean bond distance of 2.283 (6) Å may be compared to those in $[Fe_4S_4(SR)_4]^{2-,3-}$ clusters such as $[Fe_4S_4(SCH_2Ph)_4]^{2-}$ (2.251 (3) Å[37]) and **3** (2.315 (2) Å[25]). Inasmuch as these distances respond to changes in the metal oxidation state in Fe_4Q_4 clusters and are typical values,[35,36] the bond length of **10** suggests a mean iron oxidation state in the range $Fe^{2.50+}$ to $Fe^{2.25+}$ with bias toward the lower end. The situation with **11** (2.282 (2) Å) is the same, the terminal bond lengths in **5** and **7** being 2.264 (8) and 2.298 (7) Å,[26] respectively.

The nickel atom resides in a trigonally distorted tetrahedral coordination site with the mean bond angles P–Ni–Q = 113 (2)°/111 (3)° and Q–Ni–Q = 105.8 (7)°/108.3 (9)° (Q = S/Se). The Ni–P distances are indistinguishable in the two clusters and, as Fe–SR distances, might be considered to convey the effective oxidation state of nickel. The value of 2.18 Å is among the shortest such distances reported. It is substantially shorter than those in the Ni(II,I) complexes $[Ni(PPh_3)X_3]^{1-}$ (2.28–2.35 Å),[38] $Ni(PPh_3)_2X_2$ (2.32–2.34 Å),[39] and $Ni(PPh_3)_3Br$ (2.30–2.33 Å),[40] and marginally shorter than typical distances in Ni(0) compounds such as $Ni(PPh_3)_2(CO)_2$ (2.22 Å)[41a] and $Ni(PPh_3)_3(PhCN)$ (2.19 Å).[41b] All of these molecules are tetrahedral. We observe that the Ni–P distance is comparable to the mean value in the cluster $Ni_8S_5(PPh_3)_7$ (2.16 Å) ($Ni^{1.25+}$, 2.16 (1) Å[42]) but shorter than in other Ni–S–PPh_3 clusters ($Ni^{(1.5-2)+}$, 2.23–2.27 Å).[43] Comparisons within the foregoing set are complicated by steric interactions between differing numbers of the bulky PPh_3 ligands and, in clusters, by Ni–Ni bonding and departures from tetrahedral stereochemistry. We decline to infer a nickel oxidation state from such a comparison and show below that any charge distribution involving the Ni(0) oxidation state, which in mononuclear species comes closest to the observed Ni–P distance, is improbable. Further, no divalent ion has yet been observed to bind to the $[Fe_3S_4]^{1+}$ cluster in proteins (Figure 1), because the electrophilic demands of three Fe(III) subsites render the sulfur atoms insufficiently basic. Nickel(0) is even less likely to fulfill this binding function.

(b) $[NiFe_3Se_4(SEt)_4]^{3-}$. The compound $(Et_4N)_3$[**12**] is isomorphous with $(Et_4N)_3$[**7**]. Determination of its structure served to prove the cubane-type cluster stereochemistry. However, disorder prevented the identification of a specific nickel subsite within the cluster. Consequently, neither a depiction of the cluster structure, which is unexceptional, nor a table of metric parameters is presented here.[27] The average M–M and M–Se distances in

(35) Berg, J. M.; Holm, R. H. In *Iron–Sulfur Proteins*; Spiro, T. G., Ed.; Wiley-Interscience: New York, 1982; Chapter 1.

(36) (a) Carney, M. J.; Papaefthymiou, G. C.; Spartalian, K.; Frankel, R. B.; Holm, R. H. *J. Am. Chem. Soc.* **1988**, *110*, 6084 and references therein. (b) Carney, M. J.; Papaefthymiou, G. C.; Frankel, R. B.; Holm, R. H. *Inorg. Chem.* **1989**, *28*, 1497 and references therein.

(37) Averill, B. A.; Herskovitz, T.; Holm, R. H.; Ibers, J. A. *J. Am. Chem. Soc.* **1973**, *95*, 3523.

(38) (a) Brenndorfer, M.; Brune, H. A.; Debaerdemaeker, T.; Hemmer, R. *Z. Naturforsch.* **1985**, *40b*, 357. (b) Hanton, L. R.; Raithby, P. R. *Acta Crystallogr.* **1980**, *36B*, 2417. (c) Taylor, R. P.; Templeton, D. H.; Horrocks, W. D., Jr. *Inorg. Chem.* **1968**, *7*, 2629.

(39) (a) Corain, B.; Longato, B.; Angeletti, R.; Valle, G. *Inorg. Chim. Acta* **1985**, *104*, 15. (b) Brammer, L.; Stevens, E. D. *Acta Crystallogr.* **1989**, *45C*, 400. (c) Jarvis, A. J.; Mais, R. H. B.; Owston, P. G. *J. Chem. Soc. A* **1968**, 1473.

(40) Mealli, C.; Dapporto, P.; Sriyunyonwat, V.; Albright, T. A. *Acta Crystallogr.* **1983**, *C39*, 995.

(41) (a) Krüger, C.; Tsay, Y.-H. *Cryst. Struct. Commun.* **1974**, *3*, 455. (b) Bassi, I. W.; Benedicenti, C.; Calcaterra, M.; Rucci, G. *J. Organometal. Chem.* **1976**, *117*, 285.

(42) Fenske, D.; Hachgenei, J.; Ohmer, J. *Angew. Chem., Int. Ed. Engl.* **1985**, *24*, 706.

(43) (a) Ghilardi, C. A.; Innocenti, P.; Midollini, C.; Orlandini, A. *J. Chem. Soc., Dalton Trans.* **1985**, 2209. (b) Fenske, D.; Hachgenei, J.; Ohmer, J. *Angew. Chem., Int. Ed. Engl.* **1985**, *24*, 705. (c) Fenske, D.; Fleischer, H.; Krautscheid, H.; Magull, J. *Z. Naturforsch.* **1990**, *45*, 127.

Table III. Electronic Properties of $[NiFe_3Q_4(PPh_3)(SEt)_3]^{2-}$

property	9	10
Curie–Weiss range,[a] K	5–40	5–70
C, emu K/G[b]	1.91	1.94
θ, K	−3.17	−1.31
S	3/2	3/2
μ_{eff}, μ_B	3.90	3.95
g[c,d]	4.36, 3.26, 1.86	4.96, ---, 1.30
D, cm^{-1}	3.9	5.7
$\lvert E/D\rvert$	0.05	0.18
δ, mm/s (4.2 K)[f]	0.47	[e]
ΔE_Q, mm/s (4.2 K)[f]	−0.90	[e]

[a] Curie–Weiss law: $1/\chi^M = C(T-\theta)$. [b] $C = 1.88$ for $S = {}^3/_2$. [c] Cf. Figure 8. [d] Data for the $[NiFe_3S_4]^{1+}$ cluster in *P. furiosus* Fd:[12] g = 4.9, 3.0, 1.8, $\lvert E/D\rvert = 0.18$ (upper doublet). Cyanide-bound cluster: g = 4.4, 3.7, 1.9; $D > 0$, $E/D = 0.06$ (lower doublet). [e] Not measured. [f] Reference 20.

12 at 193 K are 2.80 (4) and 2.43 (2) Å, compared to 2.782 and 2.413 (9) Å in **7** at 170 K.[26] The core volume of **12** calculated from atomic coordinates is 10.76 Å^3, the same as that of **5** (10.75 Å^3) but about 5% smaller than that of **7** (10.92 Å^2).

Ground States and Electron Distribution. Relevant electronic properties of clusters **9** and **10** are collected in Table III. As a first approximation to charge distribution in the $[NiFe_3Q_4]^{1+}$ core, the four possibilities in series 5 are considered. One of these, distribution 5a, can be dismissed immediately inasmuch as the tetrahedral configuration at the nickel subsite is inconsistent with the planar/tetragonal stereochemistry of Ni(III),[44] to which there are no exceptions. Furthermore, the isomer shift $\delta = 0.47$ mm/s of **9**[20] is much different from that of protein-bound $[Fe_3S_4]^{1+}$ in series 6,[45] eliminating distribution 5d as a possibility.

(a) $Ni^{3+} + [Fe_3S_4]^{2-}$ (c) $Ni^{1+} + [Fe_3S_4]^{0}$ (5)

(b) $Ni^{2+} + [Fe_3S_4]^{1-}$ (d) $Ni^{0} + [Fe_3S_4]^{1+}$

$[Fe_3S_4]^{1+}$	$[Fe_3S_4]^{0}$	$[Fe_3S_4]^{1-}$	(6)
0.27 (Fe^{3+})	0.42 ($Fe^{2.67+}$)	0.56 ($Fe^{2.33+}$) mm/s	

The magnetic susceptibilities of clusters **9** and **10** were examined in the 5–300 K interval at 5 kOe, and the magnetization behavior of **10** was examined at 2–300 K in applied fields up to 50 kOe. Plots of the data for **10** are shown in Figure 7; the nested curves at different applied fields indicate that the zero field splitting parameter $D \neq 0$. At low temperatures and high magnetic fields, the cluster exhibits classical saturation magnetization behavior for a $S = {}^3/_2$ system with a large zero field splitting. Acceptable fits of the magnetization data to the spin Hamiltonian of eq 7 were

$$\mathbf{H} = D[S_z^2 - S(S+1)/3] + E(S_x^2 + S_y^2) + g\mu_B H\cdot S \quad (7)$$

obtained with the parameters in Table III. In the low-temperature region, the magnetic susceptibilities follow the Curie–Weiss law with Curie constants consistent with an $S = {}^3/_2$ ground state. At higher temperatures, the susceptibilities deviate from a $1/T$ behavior in a manner consistent with the population of states of higher spin. The deviation of **10** has been modeled using the spin Hamiltonian 7 to which has been added the spin coupling term $JS_1\cdot S_2$ with $S_1 = {}^5/_2$ ($[Fe_3S_4]^{1-}$) and $S_2 = 1$ (Ni^{2+}) antiferromagnetically coupled to give an $S = {}^3/_2$ ground state. The best fit was obtained with $J = 134$ cm^{-1} and the other parameters unchanged. Attempted fits based on $S_1 = 2$ ($[Fe_3S_4]^{0}$] and $S = {}^1/_2$ (Ni^{1+}) were much less satisfactory. The spin states of Fe_3S_4

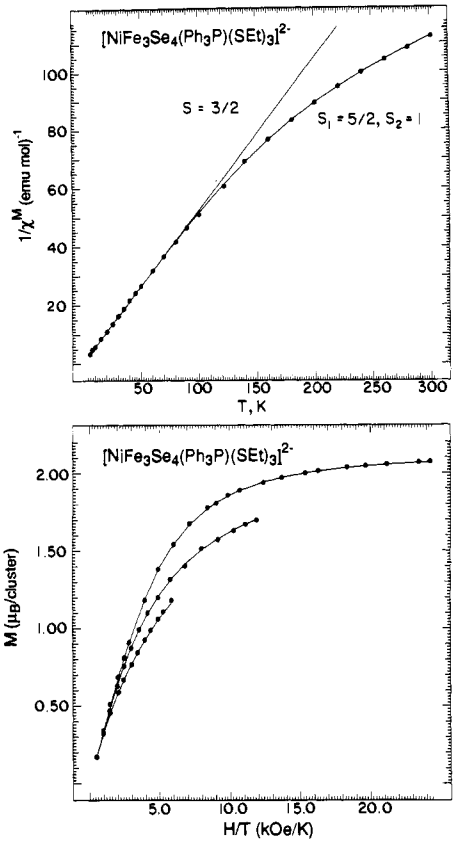

Figure 7. Magnetic properties of cluster **10**. The upper plot shows the temperature dependence of the inverse molar susceptibility; the solid line through the linear data points is a fit to the Curie–Weiss law using the parameters in Table III, and the curved portion is a fit based on the antiparallel coupling of the two indicated spins (see text). The lower plot displays the magnetization vs H/T at, from top to bottom, H = 50, 25, and 12.5 kOe; solid lines are fits to the data using the parameters of Table III.

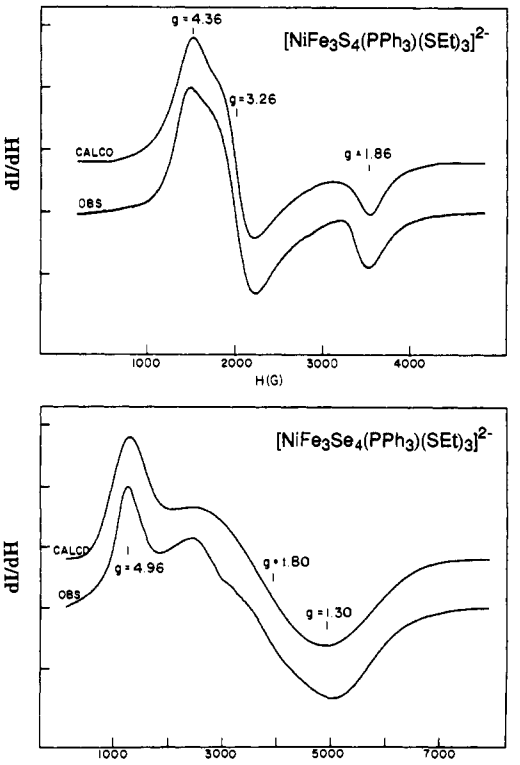

Figure 8. X-band EPR spectra of clusters **9** (upper) and **10** (lower) at 10 K in acetonitrile solutions together with spectra simulated using the indicated g values.

(44) (a) Nag, K.; Chakravorty, A. *Coord. Chem. Rev.* **1980**, *33*, 87. (b) Haines, R. I.; McAuley, A. *Coord. Chem. Rev.* **1981**, *39*, 77. (c) Lappin, A. G.; McAuley, A. *Adv. Inorg. Chem.* **1988**, *32*, 241.

(45) (a) Kent, T. A.; Dreyer, J.-L.; Kennedy, M. C.; Huynh, B. H.; Emptage, M. H.; Beinert, H.; Münck, E. *Proc. Natl. Acad. Sci. U.S.A.* **1982**, *79*, 1096. (b) Emptage, M. H.; Kent, T. A.; Huynh, B. H.; Rawlings, J.; Orme-Johnson, W. H.; Münck, E. *J. Biol. Chem.* **1980**, *255*, 1793. (c) Huynh, B. H.; Moura, J. J. G.; Moura, I.; Kent, T. A.; LeGall, J.; Xavier, A. V.; Münck, E. *J. Biol. Chem.* **1980**, *255*, 3242. (d) Surerus, K. K.; Kennedy, M. C.; Beinert, H.; Münck, E. *Proc. Natl. Acad. Sci. U.S.A.* **1989**, *86*, 9846.

Table IV. ^{1}H Isotropic Shifts of $[NiFe_3Q_4(SEt)_3L]^{z-}$ Clusters in CD_3CN Solutions at 297 K

		$(\Delta H/H_o)_{iso}$,[a] ppm					
	L	CH_2	CH_3	L	no. of equiv	% convsn	byproduct
9	PPh_3	−55.7	−2.92	−1.79 (o-H), +3.06 (m-H), −3.46 (p-H)			
10	PPh_3	−60.5	−2.91	−1.97 (o-H), +3.58 (m-H), −3.82 (p-H)			
11	EtS^-	−55.7	−4.63	+41.9 (CH_2)[b]			
12	EtS^-	−60.8	−5.06	+44.9 (CH_2)[b]			
14	$P(OMe)_3$	−56.3	−3.46	−0.24	5	95	
15	PEt_3	−55.6	−3.47	+38.5 (CH_2), −1.13 (Me)	5	99	
16	PCy_3	−54.3	−2.53	+36.5 (PCH)[c]	>4	80	7% 4
17	PPh_2Me	−56.2	−3.21	+28.0 (Me), −3.10 (o-H), +3.45 (m-H), −3.79 (p-H)	10	90	5% 4
18	$PPhMe_2$	−56.4	−3.50	+31.1 (Me), −3.40 (o-H), +3.85 (m-H), −4.16 (p-H)	8	85	5% 4
19	dmpe	−119	−15.7	−14.0 (CH_2), −2.98 (Me)	1	70	16% 4
20	dmpb	−121	−15.9	−4.65, −8.45 (ring), −2.65 (Me)	1	98	
21	CN^-[d]	−56.3	−4.35		2	70	14% 6
22	*t*-BuNC	−56.7	−4.17	+0.41	8	90	5% 4
23	PPh_3	e		−2.13 (o-H), +3.10 (m-H), −3.70 (p-H)	3	82	18%[f]

[a] $(\Delta H/H_o)_{iso} = (\Delta H/H_o)_{dia} - (\Delta H/H_o)_{obs}$; diamagnetic references are free thiols, phosphines, and t-BuNC. [b] Me assignment uncertain. [c] Remaining Cy protons, complex multiplet. [d] Slow reaction. [e] Fe–SPh: +10.5 (o-H), −5.77 (m-H), +9.79 (p-H). [f] $[Fe_4S_4(SPh)_4]^{2-}$.

fragments in Figure 1 have been determined by magnetic measurements[46] or by spectroscopic methods.[19,45-47]

The EPR spectrum of cluster **9** in Figure 8 (upper) is consistent with a rhombically split $S = {}^3/_2$ ground state and $D > 0$ and has been simulated[48] with g values of 4.36, 3.26, and 1.86. The spectrum of cluster **10** is somewhat different and has also been simulated as shown in Figure 8 (lower) with $S = {}^3/_2$. Simulations of 10 K spectra were insufficiently sensitive to values of $|E/D|$ to determine unique values. The values of D and $|E/D|$ in Table III are those from the magnetic analysis. While the EPR spectrum of **9** resembles more closely the cyanide-treated form of the $NiFe_3S_4$ species of *P. furiosus* Fd rather than that generated in the absence of cyanide,[12] the spectrum provides a direct link between the synthetic clusters of the proven structure and the protein-bound cluster. They are clearly isoelectronic with the same ground state; consequently, it is essentially certain that the protein-bound cluster has the cubane-type structure with a closely related electron distribution. Collectively, analysis of the magnetic data of **10**, Fe–SR terminal distances of **9** and **10**, and the isomer shift of **9** clearly favor distribution 5b over 5c.

^{1}H Isotropic Shifts. The $S = {}^3/_2$ ground state of the $[NiFe_3Q_4]^{1+}$ clusters induces substantial isotropic shifts, which are evident in the spectra of Figures 4 and 5. Shifts of clusters **9–12** are set out in Table IV together with those of other species **14–23** which have been produced by ligand substitution reactions (vide infra). The shifts reveal characteristic features of dominant contact interactions at iron and nickel subsites: (i) strongly attenuated methyl vs methylene shifts of the same sign for Fe–SEt ligands; (ii) alternation in sign of Fe–SPh (**23**) and Ni–PPh shifts (**9**, **10**, **17**, **18**); (iii) opposite temperature dependencies of shifts of opposite sign; (iv) larger shifts of **10**/**12** vs **9**/**11**. These are just the properties displayed by the more conventional $[Fe_4Q_4(SR)_4]^{2-,3-}$ clusters,[26,49-51] indicating that upon substitution of a nickel atom into the core, spin delocalization persists as the principal means of effecting isotropic shifts, at least in the $[NiFe_3Q_4]^{1+}$ oxidation state.

The most striking feature of the isotropic shifts is the *opposite* signs of Fe–SCH_2 (downfield) and Ni–SCH_2 (upfield) shifts of identical ligands in clusters **11** and **12**. Further, the shift patterns of Ni–PPh and Ni–PMe protons are opposite to those of tetrahedral $Ni(PPh_3)_2X_2$[52] and $Ni(PPh_2Me)_2X_2$[53] complexes, for which the contact shift mechanism dominates. This behavior follows from antiferromagnetic coupling of the spins of the $[Fe_3S_4]^{1-}$ ($S = {}^5/_2$) and Ni^{2+} ($S = 1$) cluster fragments. The larger magnetic moment is aligned parallel to the magnetic field, leading to ligand → metal antiparallel spin transfer into the local half-filled d-type orbitals of Fe(II,III) and placement of positive (α) spin in the S 3p-type orbitals. The situation is reversed at the nickel subsite where the spin is antiparallel to the applied field. Here spin transfer places negative (β) spin at the phosphorus atom, likely in the lone pair (σ) orbital. Spin is delocalized owing to the nonorthogonality of the spin-containing sulfur or phosphorus orbital with phenyl π-orbitals in the odd-alternate systems simply represented by canonical forms **24** and **25**. From elementary

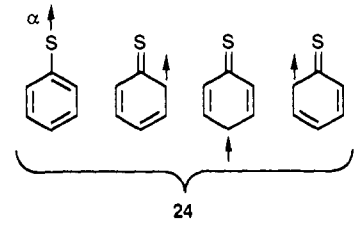

24

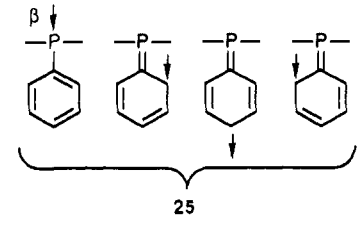

25

contact shift considerations[49,52] ($(\Delta H/H_o)_{iso} = -(\text{constant})A_i/T$) and the McConnell equation ($A_i = Q_{CH}\rho_{Ci}$, $Q_{CH} \approx -23$ G), positive spin density (ρ_{Ci}) will afford a positive contact shift of proton H_i, and the converse. In mononuclear tetrahedral Ni(II) complexes such as $Ni(PPh_2Me)_2Cl_2$[53] and $[Ni(SPh)_4]^{2-}$,[54] where the magnetic moment of the $S = 1$ ground state tends to align with the applied field, *o*-H and *p*-H isotropic shifts are positive and Me and *m*-H shifts are negative.

Reactivity. (a) Ligand Substitution. Unlike all previous heterometal cubanes **1**, the subsites of $NiFe_3Q_4$ clusters involve kinetically labile metals with the same stereochemistry. However,

(46) (a) Day, E. P.; Peterson, J.; Bonvoisin, J. J.; Moura, I.; Moura, J. J. G. *J. Biol. Chem.* **1988**, *263*, 3684. (b) Weigel, J. A.; Srivastava, K. K. P.; Day, E. P.; Münck, E.; Holm, R. H. *J. Am. Chem. Soc.* **1990**, *112*, 8015.

(47) Conover, R. C.; Kowal, A. T.; Fu, W.; Park, J.-B.; Aono, S.; Adams, M. W. W.; Johnson, M. K. *J. Biol. Chem.* **1990**, *265*, 8533.

(48) Simulations were performed with the program QPOW by R. L. Belford, A. M. Maurice, and M. J. Nigles: (a) Nigles, M. J. Ph.D. Thesis, University of Illinois, Urbana, 1979. (b) Maurice, A. M. Ph.D. Thesis, University of Illinois, Urbana, 1980.

(49) (a) Holm, R. H.; Phillips, W. D.; Averill, B. A.; Mayerle, J. J.; Herskovitz, T. *J. Am. Chem. Soc.* **1974**, *96*, 2109. (b) Reynolds, J. G.; Laskowski, E. J.; Holm, R. H. *J. Am. Chem. Soc.* **1978**, *100*, 5315.

(50) Bobrik, M. A.; Laskowski, E. J.; Johnson, R. W.; Gillum, W. O.; Berg, J. M.; Hodgson, K. O.; Holm, R. H. *Inorg. Chem.* **1978**, *17*, 1402.

(51) Feature iv has been shown to arise from the larger paramagnetism of selenium vs sulfur clusters,[26,49] as expected for contact interactions.

(52) (a) LaLancette, E. A.; Eaton, D. R. *J. Am. Chem. Soc.* **1964**, *86*, 5145. (b) LaMar, G. N.; Horrocks, W. D., Jr.; Allen, L. C. *J. Chem. Phys.* **1964**, *41*, 2126. (c) Pignolet, L. H.; Horrocks, W. D.; Holm, R. H. *J. Am. Chem. Soc.* **1970**, *92*, 1855. (d) LaMar, G. N.; Sherman, E. O. *J. Am. Chem. Soc.* **1970**, *92*, 2691.

(53) LaMar, G. N.; Sherman, E. O.; Fuchs, G. A. *J. Coord. Chem.* **1971**, *1*, 289.

(54) Rosenfield, S. G.; Armstrong, W. H.; Mascharak, P. K. *Inorg. Chem.* **1986**, *25*, 3014.

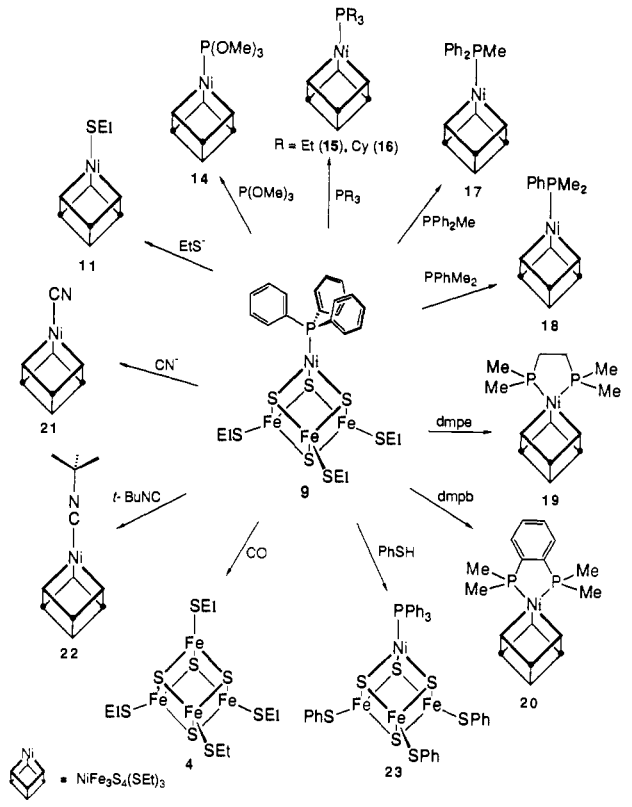

Figure 9. Schematic representation of the substitution reactions of cluster 9 in acetonitrile solution; some of these reactions produce Fe_4S_4 cluster **4** or **6** as a byproduct (cf. Table IV).

in a cluster such as **9**, regiospecific reactions at the nickel subsite are strongly favored inasmuch as PPh_3 is a far superior leaving group to ethanethiolate. The reactions of **9** displayed in Figure 9 and summarized in Table IV were monitored by ^1H NMR in acetonitrile solutions. Reaction was indicated by the appearance of free PPh_3 resonances, and isotropic shifts facilitated product identification. Thus, **9** reacts with excess $P(OMe)_3$ and more basic *tert*-phosphines to afford the products **14–18** in 80% or higher in situ yields. With chelating diphosphines, clusters **19** and **20** were formed, the latter in essentially quantitative yields. The Fe–SCH_2 isotropic shifts of ca. −120 ppm are about twice as large as those of any other cluster in Table IV and the largest we have observed for this group in any cubane cluster. This suggests a spin state with $S > {}^3/_2$ for the Fe_3S_4 fragment, a matter currently under investigation.

In other reactions, cluster **9** was partially converted with excess ethanethiolate to **11**, which was also formed in the preparative system (Figure 2). Reaction with 2 equiv of cyanide gave **21** (70%), while treatment with 8 equiv of *t*-BuNC resulted in the formation of **22** (90%). In experiments also monitored by ^1H NMR, 10 mM solutions of **10** in acetonitrile were treated with 1–4 equiv of CO in NMR tubes which were then vigorously shaken. After 30 min with 4 equiv, 50% of the original cluster was removed, and after 18 h the cluster was absent. Within this range of equivalents and reaction times, the only detectable product was the Fe_4Se_4 cluster **5**. In a control experiment, a 10 mM solution of **5** did not react with 8 equiv of CO over 1 h. Similarly, exposure of **9** in acetonitrile solutions to 2–4 equiv of carbon monoxide for 18 h resulted in the formation of the Fe_4S_4 cluster **4** as the only product identifiable by NMR.[55] Indeed, this cluster or its reduced form **6** frequently appear as secondary products in other ligand substitution reactions under mild conditions (Table IV) as well as in solutions exposed to dioxygen or containing protic

(55) We surmise that binding of CO to the nickel subsite renders it reducible to (unidentified) Ni^0–CO–PPh_3 species with attendant core degradation and formation of **4**, well-known to be a thermodynamic sink in Fe–S–SR cluster assembly systems.

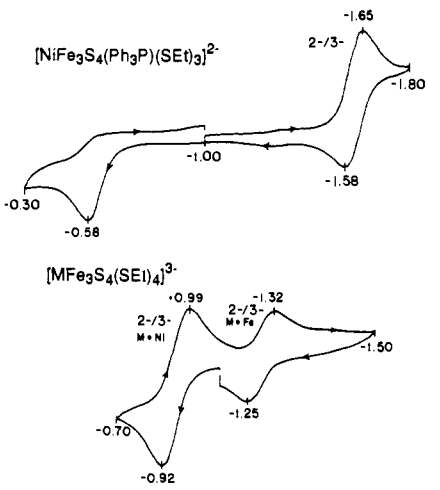

Figure 10. Cyclic voltammograms of cluster 9 (upper) and a mixture of **6** and **11** in acetonitrile solutions at 50 mV/s; peak potentials vs SCE are indicated.

impurities. From such observations, we conclude that $[NiFe_3S_4]^{1+}$ clusters, at least with the terminal ligands used here, are not nearly as robust as $[Fe_4S_4]^{2+}$ clusters and must be handled accordingly.

Treatment of **9** with 3 equiv of PhSH resulted in the expected formation of the Fe-substituted cluster **23**, but also with some decomposition to $[Fe_4S_4(SPh)_4]^{2-}$ (18%). Other ligands tested did not react at either the iron or the nickel subsites.[56]

(b) Redox. Cyclic voltammograms of clusters **9** and **6**/**11** are shown in Figure 10. The former shows a chemically reversible reduction at $E_{1/2} = -1.62$ V and an irreversible oxidation at $E_{pa} = -0.58$ V. The corresponding values for **10** are −1.49 and −0.46 V. The comparative couples 8 and 9 provide the first measure

$[NiFe_3Q_4(SEt)_4]^{2-/3-}$:

$$E_{1/2} = -0.95\ (Q = S),\ -0.93\ V\ (Q = Se) \qquad (8)$$

$[Fe_4Q_4(SEt)_4]^{2-/3-}$:

$$E_{1/2} = -1.31\ (Q = S),\ -1.28\ V\ (Q = Se) \qquad (9)$$

of the effect of a heterometal atom on the potentials of clusters known to have identical charges and terminal ligands. The effect is quite substantial, the $[NiFe_3Q_4]^{2+}$ clusters being more susceptible to reduction by some 0.35 V than $[Fe_4Q_4]^{2+}$ clusters.[57] Attempts to generate the $[NiFe_3S_4]^{2+}$ oxidation level by controlled potential electrolysis of **9** led to cluster decomposition. This level will be sought in more stable clusters.

Summary. The following are the principal findings and conclusions of this investigation.

(1) Clusters **9–12** containing the cubane-type $NiFe_3Q_4$ core (Q = S, Se) can be prepared from the linear trinuclear Fe(III) clusters $[Fe_3Q_4(SR)_4]^{3-}$ and a reduced nickel source ($Ni(PPh_3)_4$) in a process involving *reductive rearrangement* of the cluster to a cuboidal form and (concerted) capture of a nickel atom.[58] The process, which can be likened to an inner-sphere electron-transfer reaction with a persistent intermediate, may be of some general

(56) No reaction occurred upon addition of ≥20 equiv of pyridine, 2,2-bipyridyl, *N,N,N',N'*-tetramethylethylenediamine or 1,4,7-trithiacyclonane. Addition of 1–3 equiv of $KHB(pz)_3$ or 1,4,7-triazocyclononane caused decomposition and formation of an insoluble black solid. These observations refer to acetonitrile solutions of **9** at room temperature.

(57) Similarly, the difference in potentials of the $[CoFe_3S_4(tibt)_4]^{2-/3-}$ [21] and $[Fe_4S_4(tibt)_4]^{2-/3-}$ couples (−1.09 − (−1.27) = 0.18 V in acetonitrile) reveals a relative destabilization of the oxidized form of the heterometal cluster toward reduction. This behavior does not hold with the $[MFe_3S_4]^{2+/1+}$ couples of reconstituted *P. furiosus* Fd;[15] potentials for the M = Zn and Cd species are substantially more negative than for the M = Fe protein.

(58) The reductive rearrangement reaction is related to the formation of VFe_3S_4 cubane clusters from linear $[Cl_2FeS_2VS_2FeCl_2]^{3-}$ and Fe(II);[2,59] here reduction of V(V) induces structural rearrangement of a cuboidal fragment that captures an iron atom. These reactions differ from reactions 1 and 2, and one method afforded **13**,[21] in which a ligand, and not the heterometal, is the reductant.

(59) Kovacs, J. A.; Bashkin, J. K.; Holm, R. H. *Polyhedron* **1987**, *6*, 1445.

utility inasmuch as $CoFe_3S_4$ clusters related to **13** are accessible using Co(I) reactants.[22]

(2) The cluster products **9**, **10**, and **12** of (1) have cubane-type $[NiFe_3Q_4]^{1+}$ cores that differ only slightly in bond distances and volumes from the more familiar $[Fe_4S_4]^{2+,1+}$ clusters. One consequence of structural near-identity is the isomorphism and virtual inseparability of salts of $[Fe_4Q_4L_4]^{z-}$ and $[MFe_3Q_4L_4]^{z-}$ with the same cation (e.g., **6**/**11**). Consequently, reactions that afford heterometal subsite differentiation present an advantage if both MFe_3Q_4 and Fe_4Q_4 clusters are formed in the same system.

(3) Collective structural, magnetic, ^1H NMR, and Mössbauer[20] results support the fragment formulation $[Fe_3Q_4]^{1-}$ ($S = {}^5/_2$) and Ni^{2+} ($S = 1$) as the zeroth-order description of charge distribution and antiparallel spin coupling between fragments as the origin of the $S = {}^3/_2$ ground state. This mode of spin coupling results in oppositely signed isotropic (contact) shifts of identical ligands at iron and nickel subsites.

(4) Subsite-differentiated cluster **9** undergoes a variety of regiospecific substitution reactions to afford species with ligands such as phosphines, cyanide, and isonitrile at the nickel subsite. Detection of these reactions, which are sometimes accompanied by the formation of Fe_4S_4 cluster **4** as a byproduct, is facilitated by the large isotropic shifts afforded by the $S = {}^3/_2$ ground state.

(5) The protein-bound $NiFe_3S_4$ species of *P. furiosus* Fd and synthetic $[NiFe_3S_4]^{1+}$ clusters (represented by **9**) have similar EPR spectra and the same ground state and thus are isoelectronic. It is entirely probable that the former has the cubane-type structure with a tightly bound nickel atom, as demonstrated for the synthetic clusters.

Seven heterometal cubane-type MFe_3S_4 clusters (M = V, Nb, Mo, W, Re, Co, Ni) have now been synthesized, some in several different oxidation states.[19] It appears that only lack of experimental ingenuity or of cluster stability will prevent incorporation of practically all metals into these clusters. Given the prevalence of Fe_4S_4 clusters, and detection of an increasing number of cuboidal Fe_3S_4 clusters, in many proteins and enzymes, a possible biological role for MFe_3S_4 species must be actively entertained. Our initial investigation of this matter with respect to one nickel-containing carbon monoxide dehydrogenase, by X-ray absorption spectroscopy, has shown that the $NiFe_3S_4$ cubane cluster is absent.[60] We are continuing our studies of MFe_3Q_4 clusters and their possible biological relevance. A forthcoming report will provide additional examples of reductive rearrangement reactions for the synthesis of these clusters.

Acknowledgment. This research was supported by NIH Grant GM 28856. X-ray equipment was obtained through NIH Grant 1 S10 RR 02247. We thank Russell Larsen for experimental assistance. EPR analysis software was furnished by the Illinois EPR Research Center, NIH Division of Research Resources Grant RR 01811.

Supplementary Material Available: Crystallographic data for the three compounds in Table I, including tables of intensity collections, atom and thermal parameters, bond distances and angles, and calculated hydrogen atom positions (21 pages); listings of calculated and observed structure factors (75 pages). Ordering information is given on any current masthead page.

(60) Tan, G. O.; Ensign, S. A.; Ciurli, S.; Scott, M. J.; Hedman, B.; Holm, R. H.; Ludden, P. W.; Korszun, Z. R.; Stephens, P. J.; Hodgson, K. O. *Proc. Natl. Acad. Sci. U.S.A.*, in press.

Transition-State Structural Variation in a Model for Carbonyl Reduction by Lactate Dehydrogenase: Computational Validation of Empirical Predictions Based upon Albery–More O'Ferrall–Jencks Diagrams

John Wilkie and Ian H. Williams*

Contribution from the School of Chemistry, University of Bath, Bath BA2 7AY, UK.
Received July 29, 1991

Abstract: The transition-state (TS) structure for reduction of formaldehyde by dihydropyridine (hydride donor) and imidazolium (proton donor) has been located and characterized by use of the AM1 semiempirical MO method. The hydride-transfer (HT) and proton-transfer (PT) components of this concerted reaction are kinetically coupled but dynamically uncoupled. Increasing the basicity of the imidazole moiety, by means of a suitably placed dipole of variable magnitude, leads to essentially no change in the degree of PT in the TS but to a substantial increase in the degree of HT. This computational result validates the prediction made on the basis of an Albery–More O'Ferrall–Jencks diagram. Correspondingly, the primary kinetic isotope effect (KIE) calculated for replacement of the transferring proton by a deuteron shows little change, but there is a significant increase in the magnitude of the calculated primary KIE for replacement of the transferring protide by a deuteride as the TS structure changes with increasing basicity of the imidazole moiety. This accords with the conventional view of the relationship between TS structure and the magnitude of primary KIEs.

The key to understanding of the fundamental processes of catalysis is the transition state (TS). It is of importance to know not only the nature of TS structure itself, but also the manner in which TS structure *changes* in response to changes within the reacting system and its environment, e.g., substituent and solvent effects, changes in acidity/basicity, or nucleophilicity/electrophilicity of reacting moieties. Physical organic chemists have developed empirical methods for rationalization of observed trends, as determined by experimental probes for TS structure including structure–reactivity correlations and kinetic isotope effects, and have adopted these methods for predictive purposes.[1,2] Of particular popular use has been the empirical construct known as the

(1) Thornton, E. K.; Thornton, E. R. In *Transition States of Biochemical Processes*; Gandour, R. D., Schowen, R. L., Eds.; Plenum: New York, 1978; pp 3–76.
(2) Jencks, W. P. *Chem. Rev.* **1985**, *85*, 511–527.
(3) Albery, W. J. *Prog. React. Kinet.* **1967**, *4*, 353–398.
(4) More O'Ferrall, R. A. *J. Chem. Soc. B* **1970**, 274–277.
(5) Jencks, W. P. *Chem. Rev.* **1972**, *72*, 705–718.
(6) Bruice, T. C. *Annu. Rev. Biochem.* **1976**, *45*, 331–373.

0002-7863/92/1514-5423$03.00/0